Schlessinger, J., Koppel, D., Axelrod, D., Jacobson, K., Webb, W., & Elson, E. (1976) *Proc. Natl. Acad. Sci. U.S.A. 73*, 2409.
Schlessinger, J., Axelrod, D., Koppel, D., Webb, W., & Elson, E. (1977) *Science (Washington, D.C.) 195*, 307.
Sefton, B. M., & Gaffney, B. J. (1974) *J. Mol. Biol. 90*, 343.
Singer, S. J. (1974) *Annu. Rev. Biochem. 43*, 805.
Singer, S. J., & Nicolson, G. L. (1972) *Science (Washington, D.C.) 175*, 720.
Sklar, L. A., & Dratz, E. A. (1980) *FEBS Lett. 118*, 308.
Sklar, L. A., Miljanich, G. P., Bursten, S. L., & Dratz, E. A. (1979) *J. Biol. Chem. 254*, 9583.
Struck, D. K., & Pagano, R. E. (1980) *J. Biol. Chem. 255*, 5404.
Thompson, N., & Axelrod, D. (1980) *Biochim. Biophys. Acta 597*, 155.
Windell, C. C. (1972) *J. Cell Biol. 52*, 542.
Wolf, D., Edidin, M., & Dragsten, P. (1980) *Proc. Natl. Acad. Sci. U.S.A. 77*, 2043.
Wu, E.-S., Jacobson, K., & Papaphadjopoulos, D. (1977) *Biochemistry 16*, 3936.
Wu, E.-S., Jacobson, K., Szoka, F., & Portis, A. (1978) *Biochemistry 17*, 5543.

Lateral Diffusion of Photopigments in Photoreceptor Disk Membrane Vesicles by the Dynamic Kerr Effect†

Hideo Takezoe‡ and Hyuk Yu*

ABSTRACT: The lateral diffusion of photopigment molecules in the photoreceptor disk membranes, osmotically swollen into spherical vesicles, has been investigated by dynamic Kerr effect measurements. Upon application of a rapidly reversing bipolar electric field to dilute aqueous suspensions of bovine disk membrane vesicles, the birefringence transient shows a characteristic rise and a deep dip corresponding to the first and second pulses, respectively. The birefringence transient is ascribed to the slowly induced dipole moment caused by electric field induced displacement of the photopigment distribution on the vesicular surface. The lateral translational diffusion coefficient is estimated from the time constant of the slowly induced dipole as $D = (3.3 \pm 1.2) \times 10^{-9}$ cm^2 s^{-1}. When spermine, a cationic tetraamine, is bound to the disk membrane vesicles, the relaxation time of the slowly induced dipole is shown to become longer, indicating that the birefringence mechanism is indeed due to the field-induced photopigment displacement.

The fluid mosaic model of a biomembrane accentuates the dynamic processes of the two principal components, integral proteins and phospholipids (Singer & Nicolson, 1972), on the bilayer lamellae. The processes involving integral proteins are the translational (lateral) and rotational diffusions, and these are shown to be closely related to physiological functions of a biomembrane [see, for example, a review by Edidin (1974)]. Hence, the lateral diffusion process of photopigment molecules in the photoreceptor disk membrane of the rod outer segment of vertebrate retina which is one of the first ever studied by microspectrophotometry (Poo & Cone, 1974; Liebman & Entine, 1974), has attracted significant attention in the literature. Beside this technique, there are numerous other techniques employed to study the intramembrane protein dynamics for a variety of membrane systems such as cell fusion (Frye & Edidin, 1970; Fowler & Branton, 1977; Schindler et al., 1980), spread of the fluorescent spot (Edidin & Fambrough, 1973), electrophoresis (Poo & Robinson, 1977; Poo et al., 1979), and fluorescence photobleaching–recovery (Peters et al., 1974; Jacobson et al., 1976; Schlessinger et al., 1976; Edidin et al., 1976; Smith & McConnell, 1978; Koppel, 1979; Koppel et al., 1980). Common to all of the above is the scheme of first perturbing the membrane system with optical probes and subsequently following the relaxation toward equilibrium by the dynamic process under study.

We report here a novel technique without chemical perturbation to study the lateral diffusion of photopigment molecules on the disk membrane vesicles (DMV).[1] The technique is an old one, hitherto used mostly for the rotatory diffusion of macromolecules in dilute, called the field-induced birefringence transient method or often shortened as the dynamic Kerr effect method [for a recent review, see O'Konski (1976)]. To the best of our knowledge, this is the first instance of its application to intramembrane dynamic processes. We do not imply, however, that we are the first ones to conceive of its application to the problem on hand. In fact, some 20 years ago, Tinoco & Yamaoka (1959) have suggested a possibility of studying the lateral diffusion of a mobile ion over the surface of axially symmetric macromolecules dissolved in aqueous solution. They have formulated the theory of electric field induced birefringence of macromolecules which exhibit a slowly induced dipole (SID) moment ascribed to the field-driven displacement of ions in addition to the permanent and usual induced dipole moments. By "slowly" and "usual", we mean that the time rate of inducing a dipole is comparable to and much faster than that of the global rotation of the body in question. Their theory points out that the time constant of the SID can be estimated if it is comparable to that of the

† From the Department of Chemistry, University of Wisconsin—Madison, Madison, Wisconsin 53706. *Received March 12, 1981.* Supported in part by National Institutes of Health Grant EY01483 and by a Biomedical Research Support Grant of the National Institutes of Health administered through the Graduate School of the University of Wisconsin—Madison.

‡ Permanent address: the Department of Textile and Polymeric Materials, Tokyo Institute of Technology.

[1] Abbreviations used: ROS, rod outer segment; DMV, disk membrane vesicles; SID, slowly induced dipole; EGTA, ethylene glycol bis(β-aminoethyl ether)-*N,N,N',N'*-tetraacetic acid.

0006-2960/81/0420-5275$01.25/0

rotatory relaxation of the whole macromolecule. Taking a clue from the theory, we had initiated a study to examine whether there may be a sufficient birefringence signal from dilute aqueous suspensions of DMV and if so how its decay dynamics are related to the size of DMV. Resulting from this initial inquiry, we have established that there is an enormously large field-induced birefringence due to DMV in dilute suspensions, and its dynamics are attributed to the rotatory orientation of the spherical vesicles with a rim structure (Takezoe & Yu, 1981a), which is a structural feature of DMV established earlier by its osmotic deformation behavior (Norisuye & Yu, 1977). Subsequently, we have shown that DMV have a large electric polarizability anisotropy due to the field-induced displacement of photopigments over each hemisphere of DMV separated by the rim structure which acts as the equatorial barrier (Takezoe & Yu, 1981b).

Having thus paved the way to reach the crux of our interest, we shall first present in this paper the experimental birefringence transient profiles when the applied field is a sequence of two square pulses in opposite directions such that the first square pulse is followed by the second one of opposite polarity but with equal magnitude. We shall call the sequence a "reversing pulse" in conformity with the literature. We shall then develop a theory of SID appropriate to the system of spherical DMV with the equatorial rim structure. A model of the DMV birefringence mechanism will subsequently be proposed, and finally, the lateral diffusion coefficient of photopigments will be deduced from the observed relaxation time of the SID.

Experimental Procedures

Bovine rod outer segment (ROS) disk membranes were isolated and purified from dark-adapted frozen retinae (American Stores Packing Co., Lincoln, NE) by a modified version (Norisuye et al., 1976) of the method originally employed by Smith et al. (1975). The swollen membrane vesicles were suspended in 1 mM imidazole buffer with 50 μM EGTA. The concentration of vesicles was in the range (2–8) $\times 10^9$ vesicles cm^{-3}, which was determined by monitoring the turbidity at 633 nm (Amis et al., 1981). All experiments were performed at room temperature with the bleached samples; we had not found any significant difference between bleached and unbleached samples.

The optical and detection systems for the Kerr effect measurements have been described elsewhere (Takezoe & Yu, 1981b). The electric field was applied in a reversing pulse, as explained earlier. The pulse generator was designed to supply rapidly reversing pulses of 0.1–3.2-s duration for each field direction with a variable amplitude up to 40 V/cm and with an adjustable period of 1.2–37 s. The observed birefringence is always expressed by the optical retardation, δ, in units of radians.

Results

Two experimental profiles of the electric field induced birefringence transient produced by the action of a reversing pulse are shown in Figure 1, where the time dependence of optical retardation, $\delta(t)$, normalized by its steady-state value δ_0 is displayed at two different field strengths, 3 V/cm (open circles) and 10 V/cm (closed circles). The solid curve represents a theoretical prediction to which we shall return later under Discussion. The profiles show a deep dip in each case preceded by the field-reversal point.

We now propose that the observed dip must arise from the SID in DMV. The argument in favor of the proposal goes as follows. Generally, a dip in the observed birefringence transient preceded by the field reversal is found with a molecule with the permanent dipole moment because the molecular orientation must follow the applied field direction. If the initial orientation by the first step of the reversing pulse is due to the induced polarization and if its rate is much faster than the reorientation rate of a molecule, then the orientation should remain unchanged even upon field reversal, resulting in no dip in the birefringence transient; the field reversal changes the direction of the induced polarization without perturbing the molecular orientation. On the other hand, if the induced polarization rate is comparable to that of molecular reorientation, then we should observe a dip in the transient even if the molecule in question has no permanent dipole moment (Tinoco & Yamaoka, 1959). Since we have established earlier that there is no permanent dipole moment in DMV (Takezoe & Yu, 1981b). we must conclude by virtue of the observed dip that the external electric field produces the SID. In this context, we have earlier proposed that the SID arises from the field-induced displacement of photopigment molecules. If so, the time dependence of the photopigment displacement is as slow as the global orientation of whole DMV whereby the dip can be observed. We defer until later a more quantitative treatment of the time constant and establishment of the causal relationship between the SID and photopigment displacement.

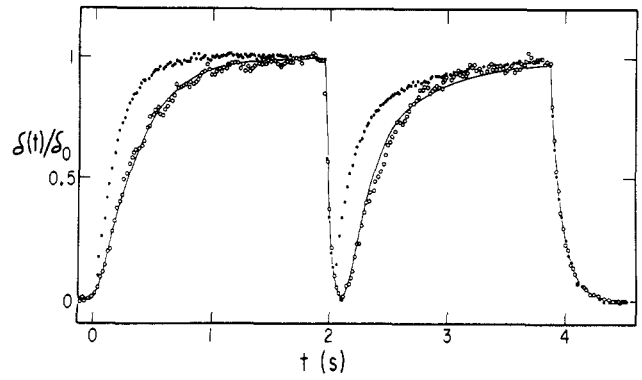

FIGURE 1: Normalized electric field induced birefringence transient, $\delta(t)/\delta_0$, by a rapidly reversing electric field. The open and filled circles refer to the results for 3 and 10 V/cm field strength, respectively. The solid curve is a theoretical prediction whose details are given under Discussion.

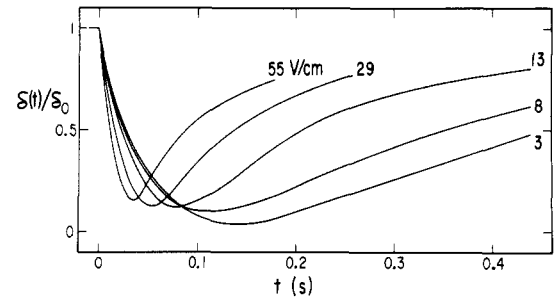

FIGURE 2: Electric field dependence of dip–recovery profiles.

Continuing on with qualitative observations of the results shown in Figure 1, it is apparent that the rise and dip profile depends on the field strength, while the decay profile does not depend on the field in the range investigated, below 70 V/cm. The dip–recovery profiles at different field strengths are shown in Figure 2 where the experimental data are replaced by smoothed curves drawn over the data points. The position of the extremum in a given profile is measured from the field-reversal point and designated as t_m, which is plotted against field strength E in Figure 3. Two different preparations of DMV are distinguished by different symbols in the figure.

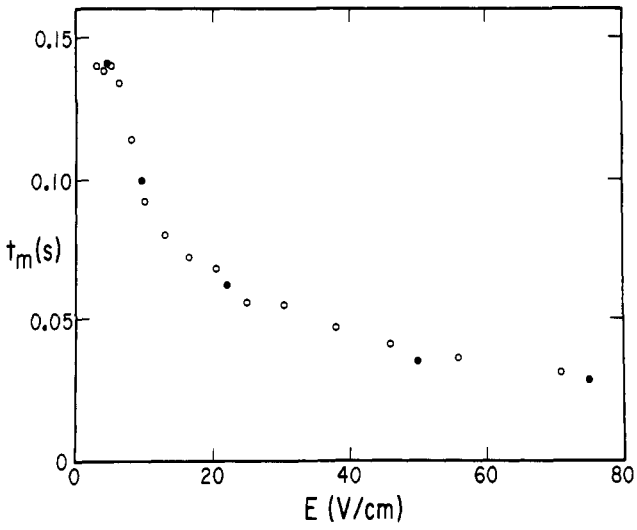

FIGURE 3: Electric field dependence of the dip position t_m. The open and filled circles refer to separate sample preparations.

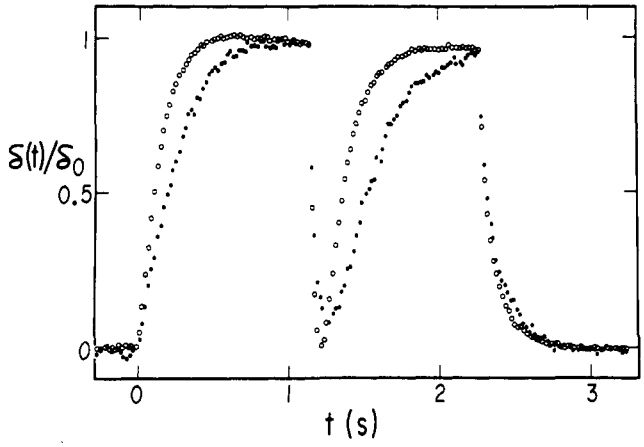

FIGURE 4: Spermine effect on birefringence transient. Open and filled circles show results for samples in 0 and 3 μM spermine, respectively.

Three observations should be made on the results presented in Figures 2 and 3: (1) the extremum position t_m varies with E and reaches the asymptotic value of 140 ms in the limit of E approaching 0; (2) the dip profiles show that the birefringence almost vanishes at the extremum, and the depth of the dip decreases slightly with increasing E; (3) the initial slope of the dip profile becomes steeper with increasing E.

In Figure 4 is displayed the last set of experimental results, where we have examined the binding effect of spermine on DMV relative to the birefringence transient. Upon addition of a small amount of spermine, the signal intensity decreases, and substantial changes appear in the rise and reverse profiles. The normalized birefringence signals $\delta(t)/\delta_0$ are plotted for the samples without spermine (open circles) and in 3 μM spermine (closed circles). The measurements were performed at 12 V/cm and with a DMV concentration of 3.7×10^9 vesicles/cm^3. The steady-state birefringence δ_0 decreases from 2.2×10^{-3} to 1.0×10^{-3} rad by addition of spermine to make its concentration 3 μM in the suspension. As for the dynamic behavior, we can clearly see that the rise becomes slower and the dip position t_m increases while the decay profile shows a little change.

Theory

The time dependence of birefringence for a dilute suspension of axially symmetric rigid objects under the influence of a reversing pulse will now be considered. For convenience, we designate the three time regimes as I, II, and III where I refers to the first pulse (rise) region, II to the second pulse (dip–recovery) region, and III to the field-free (decay) region. We shall restrict ourself to the case where the SID is the main orienting mechanism in the absence of the permanent and usual induced dipoles. We also assume that the object has a common axis of symmetry for its electrical and optical properties. Our starting point is the formulation of birefringence of axially symmetric molecules with inclusion of the SID by Tinoco & Yamaoka (1959).

We modify slightly the time-dependent polarizability originally given by Tinoco and Yamaoka for region II:

$$\alpha(t) = \alpha(1 - e^{-t/\tau}) \tag{1}$$

where τ is the SID relaxation time and α the steady-state polarizability; we need to correct the polarization formulation associated with the polarizability given by eq 1 by addition of the polarization term $\mu_a e^{-t/\tau}$ where μ_a refers to the apparent permanent dipole moment at the start of region II, i.e., $t_{II} = 0$. The bases for the modification of eq 1 are deferred to Appendix A. Thus, the energy associated with orienting torque in region I is given by

$$W = -(1/2)\alpha E^2 \cos^2\theta\,(1 - e^{-t/\tau}) \tag{2}$$

and in region II by

$$W = -\mu_a E \cos\theta\, e^{-t/\tau} - (1/2)\alpha E^2 \cos^2\theta\,(1 - e^{-t/\tau}) \tag{3}$$

where θ is the angle between the symmetry axis of the object in question and the applied field direction.

The orientational distribution function f can now be determined by solving for the diffusion equation (Tinoco, 1955; Tinoco & Yamaoka, 1959):

$$Lf - \frac{\partial f}{\partial t} = -Qf \tag{4}$$

where

$$Lf = -\frac{\Theta}{\sin\theta}\frac{\partial}{\partial\theta}\left(\sin\theta\,\frac{\partial f}{\partial\theta}\right) \tag{5}$$

$$Qf = \frac{\Theta}{kT}\left[\frac{1}{\sin\theta}\frac{\partial}{\partial\theta}\left(f\sin\theta\,\frac{\partial W}{\partial\theta}\right)\right] \tag{6}$$

where Θ is the rotatory diffusion coefficient of the symmetry axis of the object. The second-order perturbation method was used to solve for eq 4 after expanding f in terms of a power series of E. This would mean that the results can be applied to the lower field regime where the potential energy of the object in the field is comparable to or less than kT. To obtain the relation between α and μ_a, we must recall that

$$\left(\frac{\mu}{kT}\right)^2 + \frac{\alpha_1 - \alpha_2}{kT} = \frac{15n^2K_{sp}}{2\pi(g_1 - g_2)} \tag{7}$$

in the low-field regime, where K_{sp} is the specific Kerr constant and $g_1 - g_2$ is the optical anisotropy. Although we assume that there is no permanent dipole, the SID behaves like an apparent permanent dipole at the start of region II; hence

$$\left(\frac{\mu_a}{kT}\right)^2 = \frac{\alpha}{kT} \tag{8}$$

With the use of eq 8 and appropriate boundary conditions, we can determine the distribution function f and obtain the normalized birefringence transient, $\Delta n(t)$, in region II:

$$\Delta n(t) = 1 + A + B + C \tag{9}$$

where

$$A = \frac{6\Theta\tau}{6\Theta\tau - 1}(e^{-6\Theta t} - e^{-t/\tau})$$
$$6\Theta\tau \neq 1$$
$$B = -\frac{6(\Theta\tau)^2}{(2\Theta\tau - 1)(3\Theta\tau - 1)}(e^{-6\Theta t} - e^{-2t/\tau})$$
$$2\Theta\tau \neq 1; 3\Theta\tau \neq 1$$
$$C = \frac{6\Theta\tau}{2\Theta\tau - 1}[e^{-6\Theta t} - e^{-(2\Theta + 1/\tau)t}]$$
$$2\Theta\tau \neq 1$$

For the following special cases, eq 9 must appropriately be modified as follows: when $6\Theta\tau = 1$, A must be replaced by $A = -6\Theta t e^{-6\Theta t}$; when $3\Theta\tau = 1$, B must be replaced by $B = -12\Theta t e^{-6\Theta t}$; when $2\Theta\tau = 1$, $B + C$ must be replaced by $B + C = 6(e^{-6\Theta t} - e^{-4\Theta t} + \Theta t e^{-4\Theta t})$.

We now turn to the predictions of eq 9. The time-dependent birefringence in region II is plotted against the reduced time Θt in Figure 5, where the effect of the SID relaxation time τ is displayed by the profiles at different values of $6\Theta\tau$, which is the ratio of τ to the rotatory relaxation time of the symmetry axis, $1/(6\Theta)$. We check first whether our theory results in the correct limits. When $6\Theta\tau = 0$, it corresponds to the case of an induced dipole, i.e., $\tau \ll 1/(6\Theta)$, and the horizontal line without a dip is precisely that limit. When $6\Theta\tau \rightarrow \infty$, it corresponds to the case of a pure permanent dipole moment, and the profile in Figure 5 is precisely the same as the theoretical result given by Tinoco and Yamaoka for the permanent dipole orientation. Further, the initial slope of the dip, $[d(\Delta n)/dt]_{t_{II} \rightarrow 0}$, is shown to be independent of τ and given by -12Θ, which is in agreement with the case of the permanent dipole moment as it must at $t_{II} \rightarrow 0$. How the extremum position t_m and its depth Δn_m depend on τ are amplified in Figure 6 where Θt_m and Δn_m in a linear scale are plotted against $6\Theta\tau$ in a logarithmic scale. Both change monotonically with $6\Theta\tau$ and reach their respective asymptotes of $(\ln 3)/4$ and $1 - 2(3)^{1/2}$ as $6\Theta\tau$ approaches infinity. These asymptotic values are indeed in agreement with the case of a pure permanent dipole. This concludes the presentation of our theory which is a modification of that by Tinoco and Yamaoka by distinguishing regions I and II by eq 2 and 3. We emphasize here that our model is an axially symmetric body having only the SID mechanism for the electric field induced polarization. It should be noted that the rise profile of region I is also affected by $6\Theta\tau$ through eq 1 and 2 although we do not reproduce the governing birefringence expression here because it is given by Tinoco and Yamaoka. In region III, we should note that the decay profile is purely controlled by 6Θ.

Before ending this section, we call attention to the fact that the theory is only applicable in the low-field regime. The high-field effect has been dealt with by Matsumoto et al. (1970), although they did not include the slowly induced dipole. They showed that the second-order perturbation is appropriate roughly for $\beta^2 < 0.4$, where $\beta = (\mu/kT)E$. Taking account of the apparent permanent dipole moment of DMV, $\mu_a = 3.2 \times 10^{-12}$ esu (3.2×10^6 D), which is obtained from eq 8 and the experimental electric polarizability anisotropy, $\alpha_2 - \alpha_1 = 2.5 \times 10^{-10}$ cm^3 (Takezoe & Yu, 1981b), we determined that $\beta^2 = 0.4$ corresponds to $E = 2.4$ V/cm. Therefore, only the dynamic measurements in the neighborhood of 2.4 V/cm or lower in field strength can appropriately be described by this theory.

Discussion

We shall now discuss our experimental results in the context of the SID theory developed in the previous section. The most important observation to note is the appearance of a dip and subsequent recovery in region II, which is generally caused by the SID and/or by the permanent dipole moment. As we mentioned under Experimental Procedures, it was concluded that the SID must play the principal role in giving rise to a dip since we have earlier established that DMV do not have a permanent dipole moment. The observed dip position in the low-field asymptote, $t_m = 0.14$ s, also supports the existence of the SID since the expected t_m for the permanent dipole would be 0.16 s.

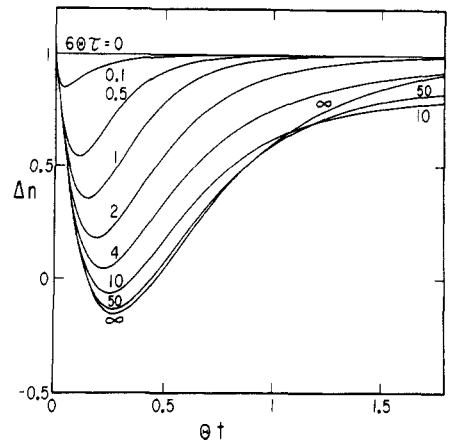

FIGURE 5: Theoretical curves of birefringence transient in reversing field region for various $6\Theta\tau$ values.

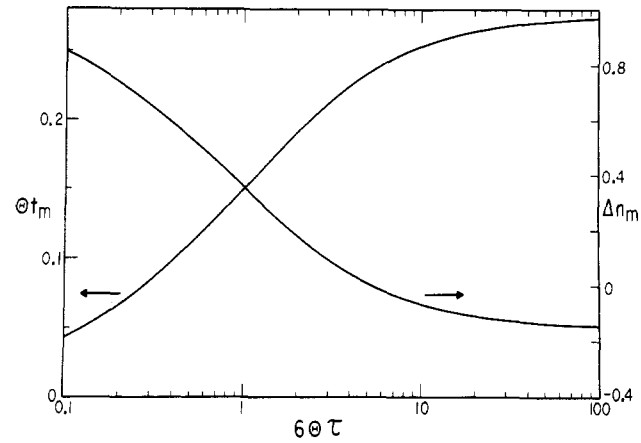

FIGURE 6: Dependence on $6\Theta\tau$ of the reduced extremum position Θt_m and the birefringence at the extremum Δn_m.

We next test whether the theory put forth in the previous section can indeed simulate the experimental transient. The solid curve drawn over the data in Figure 1 represents such a test. From the field-free decay profile of region III, we first determine $1/(6\Theta)$ as 96 ms. Assuming that the component of the SID along the transverse axis (normal to the symmetry axis) is the only important factor in the DMV orientation mechanism, we represent the transient in region I with $\tau = 300$ ms according to the expression given by Tinoco & Yamaoka (1959) and that in region II with $\tau = 500$ ms according to eq 9 as the best fit. We emphasize that the fitting is performed with a single parameter in each region. One should expect, however, that the same τ must hold for both regions. The discrepancy could have arisen from the simplifying assumption of considering only one component of the SID in the orientation mechanism. Despite such a simplification, we find it gratifying that one parameter fit to the data can simulate the result as well as shown in Figure 1. Also, the values of τ chosen to fit the data are quite reasonable inasmuch as they are comparable to or slower than the DMV rotatory relaxation

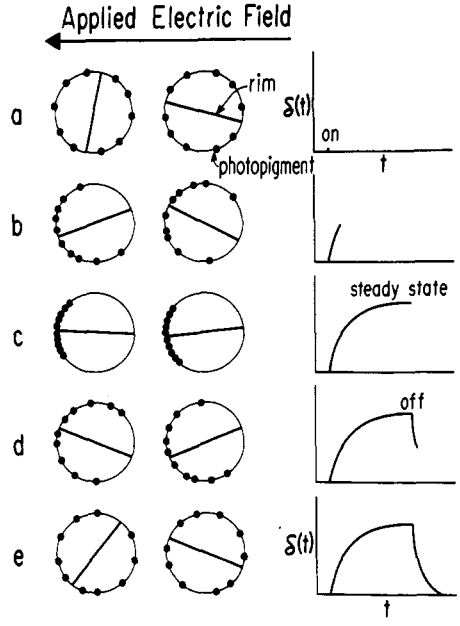

FIGURE 7: Illustration of the proposed birefringence mechanism.

time of about 100 ms; $6\Theta\tau = 3$ for region I and $6\Theta\tau = 5$ for region II.

Next, we propose a model of the birefringence mechanism which includes the essential feature of the SID without the permanent dipole moment since we have so far established that the SID alone could account for the transient results. The question is by what manner such a SID can be arisen. In order to set the stage for a plausible mechanism, we first summarize the electrooptical observations made on DMV deduced from the experiments. They are as follows:

(1) The birefringence decay in the field-free region is ascribed to the global orientation of DMV since the decay time constant is in accord with the rotatory relaxation time of a sphere with about 0.5-μm radius (Norisuye et al., 1976; Hoffman et al., 1977; Takezoe & Yu, 1981a).

(2) DMV have an equatorial rim structure (Norisuye & Yu, 1977), and it gives rise to a small but finite optical anisotropy even when DMV are in a spherical shape. Also, the dominant axis of electric polarizability is in the rim plane, and there exists a large electric polarizability anisotropy (Takezoe & Yu, 1981b).

(3) The electric field induced displacement of photopigments on the DMV surface gives rise to the large electric polarizability anisotropy, and its time constant may be comparable to the rotatory relaxation time of DMV (see below).

Based on these results, we proceed to present a model of the birefringence mechanism with use of the schematic illustration in Figure 7. (a) Prior to application of an external electric field, we have the uniform distribution of photopigments on both hemispheres and the random orientation of the rim plane relative to the field direction. (b) With the field on, the photopigment distribution is perturbed away from the uniform one. Since the rim acts as the displacement barrier, an induced dipole moment appears in the equatorial plane. At the same time, the induced dipole moment forces DMV to orient preferentially with the rim plane parallel to the applied field direction. (c) The steady state in the orientational distribution is attained after a sufficient duration with the field on although the degree of orientation depends on the field strength and the temperature. (d) When the field is off, the photopigment distribution starts to return to the unperturbed state, and at the same time, the rim plane orientation starts to recover back to the random distribution. (e) Both the photopigment distribution and rim plane orientation recover back to complete random distribution.

In light of the proposed mechanism, it is quite reasonable to attribute the SID to the field-induced displacement of photopigments on the DMV surface. Thus, we now face the task of providing evidence that such photopigment displacements are indeed taking place when the applied electric field is on. We present the experiment with spermine as such evidence. Spermine, a cationic tetravalent polyamine, is found in many different animal tissues (Cohen, 1971; Bachrach, 1973), and its binding property to DNA has been extensively studied (Tabor & Tabor, 1976; Record et al., 1978; Wilson & Bloomfield, 1979). Its binding to phospholipids, though less extensively studied, is suspected to confer to cell membranes stability against osmotic lysis (Tabor et al., 1961; Tabor & Tabor, 1976). Hence, we would expect that spermine should retard the photopigment displacement through its binding to phospholipids, rendering them more viscous through the effective electrostatic cross-linking of phospholipid molecules by its tetravalent charges. This expectation is completely borne out by the experiment. The results are shown in Figure 4 where the filled circles represent the data in 3 μM spermine while the unfilled circles stand for those of the control without spermine. Comparison of the two sets of data makes it clear that the transient in 3 μM spermine is substantially retarded in regions I and II whereas the decay profiles of the two are identical in region III, signifying that the global size of DMV is not affected by 3 μM spermine. Though not shown in Figure 4, we have also observed that the absolute value of steady-state birefringence is reduced by one-half in 3 μM spermine, indicating that spermine can also bind to photopigments so as to make them inactive for the field-induced displacement. In the context of our proposed mechanism, the neutralized photopigment molecules will not give rise to the SID; hence, the birefringence will be diminished or eventually abolished. In this respect, we might also add that the steady-state birefringence studies with divalent, trivalent, and tetravalent cations will constitute the subject of our next report.

Having thus presented evidence that the field-induced photopigment displacement takes place on the DMV surface, we finally come to the limiting case of no field. As is shown in Figure 3, the dip position in region II shifts toward longer time as the applied field strength is lowered and eventually reaches the asymptotic value of 0.14 s. It seems plausible, therefore, that the time constant in the limit of zero field should represent that of the lateral free diffusion of photopigment on the DMV surface. If so, we should be able to estimate the lateral diffusion coefficient D from the SID relaxation time τ extrapolated to the zero-field limit. In fact, one can show (see Appendix B) that D on the spherical surface of radius r is related to τ by

$$D = r^2/2\tau \qquad (10)$$

With use of the experimental results of $\tau = 0.5$ or 0.3 s, the translational diffusion coefficient of (2.4 or 4.2) $\times 10^{-9}$ cm^2 s^{-1} can be deduced through eq 10. Including the error estimate in the determination of τ, we finally arrive at $D = (3.3 \pm 1.2) \times 10^{-9}$ cm^2 s^{-1}. The same lateral diffusion coefficients of photopigment obtained by others are collected and compared in Table I. It is rather apparent that our value of $(3.3 \pm 1.2) \times 10^{-9}$ cm^2 s^{-1} is in surprisingly good agreement with those obtained by others, considering the disparate methods and systems by which all these values are obtained. It is to be noted that our value is deduced from isolated and swollen bovine disk membrane vesicles in the bleached state whereas the others were from intact whole rod cells in the unbleached state

Table I: Lateral Diffusion Coefficient of the Photopigment in Disk Membranes of the Vertebrate Retinal Rod Outer Segment

	diameter (μm)	D ($\times 10^9$ cm^2 s^{-1})	ref
bovine	1	3.3 ± 1.2	present work
frog	8	3.5 ± 1.5	Poo & Cone (1974)
	8	4.7 ± 0.9	Liebman & Entine (1974)
mudpuppy	12	3.9 ± 1.2	Poo & Cone (1974)
	13	5.5 ± 0.6	Liebman & Entine (1974)

wherein the disks were in their native state. Both groups (Poo & Cone, 1974; Liebman & Entine, 1974) made use of the microspectrophotometric technique, which is indeed different from the dynamic Kerr effect. We summarize the points of this paper as follows.

(1) With use of the SID theory developed, it is possible to render a quantitative analysis of the birefringence transients in a reversing pulse.

(2) With the SID relaxation time extrapolated to the limit of the vanishing field, the lateral diffusion coefficient of photopigment is deduced to be in good agreement with others determined by microspectrophotometry.

(3) A mechanism for the SID in the context of the birefringence model is proposed, and the retardation of the birefringence transient by spermine binding is put forth as a piece of evidence lending support to the proposed mechanism.

Acknowledgments

We acknowledge Taihyun Chang for many stimulating and valuable discussions regarding the theoretical effort presented here.

Appendix

(*A*) *Critique of Tinoco and Yamaoka for $\alpha(t)$ in Region II.* It is clear that eq 1 is not a correct form of the time dependence of polarizability in region II since $\alpha(t_{II} = 0)$ must not be 0 whereas eq 1 cannot distinguish $\alpha(t_I = 0)$ and $\alpha(t_{II} = 0)$. The incorrect form of $\alpha(t)$ in region II as used by Tinoco and Yamaoka gives rise to the following inconsistencies:

(1) The initial slope is deduced to be the same as that for the rotatory diffusion, namely, -6Θ, whereas it must be that for a permanent dipole, -12Θ.

(2) The dip position shifts with τ monotonically without limit, i.e., $t_m = \tau \ln (6\Theta\tau)/(6\Theta\tau - 1)$, whereas it must reach the asymptote of $\ln 3/(4\Theta)$.

(3) In the limit of large τ, the whole profile of region II approaches that of the decay region; $\lim_{\tau\to\infty} \Delta n_{II} = e^{-6\Theta t} = \Delta n_{III}$.

To alleviate these inconsistencies, we add another polarization term, $\mu_a e^{-t/\tau}$, as stated in the text, where μ_a is an apparent permanent dipole at $t_{II} = 0$ which depends on the field strength in region I, E_I, but not on E_{II}. Actually, even if $E_{II} = 0$, which corresponds to the decay region in the usual square pulse (without reversing) experiment, the polarization should be μ_a at $t_{II} = 0$ and decays as $e^{-t/\tau}$ while the molecule relaxes orientationally by virtue of $E_{II} = 0$.

(*B*) *Relation between the Time Constant of the SID and the Lateral Diffusion Coefficient on a Spherical Surface.* The distribution function f of the photopigment obeys the diffusion equation

$$\frac{1}{D}\frac{\partial f}{\partial t} = \nabla^2 f \tag{A1}$$

Since we are dealing with photopigments diffusing on the spherical surface, eq A1 can be written

$$\frac{1}{D}\frac{\partial f}{\partial t} = \frac{1}{r^2}\nabla_{\theta,\phi}{}^2 f \tag{A2}$$

where $\nabla_{\theta,\phi}{}^2$ is the angular part of Laplacian and r is the radius of the sphere. As usual, f can be expanded in a series of the normalized spherical harmonics $Y_{lm}(\theta,\phi)$ with coefficients C_{lm} determined by the initial condition:

$$f(\theta,\varphi,t) = \sum_{l,m} C_{lm} Y_{lm}(\theta,\phi) e^{-(D/r^2)l(l+1)t} \tag{A3}$$

The time dependence of the slowly induced dipole is proportional to $\langle \cos\theta(t)\rangle$ where θ is the angle between the equatorial plane and the radial direction to a photopigment, which is

$$\begin{aligned}\langle \cos\theta(t)\rangle &= \int_0^{\pi}\int_0^{2\pi} \cos\theta(t) f(\theta,\phi,t) \sin\theta \, d\theta \, d\phi \\ &= e^{-(2D/r^2)t} \\ &= e^{-t/\tau}\end{aligned} \tag{A4}$$

Therefore, the translational diffusion coefficient D is given by

$$D = \frac{r^2}{2\tau} \tag{A5}$$

References

Amis, E. J., Davenport, D. A., & Yu, H. (1981) *Anal. Biochem.* (in press).

Bachrach, U. (1973) *Functions of Naturally Occurring Polyamines*, Academic Press, New York.

Cohen, S. S. (1971) *Introduction to the Polyamines*, Prentice-Hall, Englewood Cliffs, NJ.

Edidin, M. (1974) *Annu. Rev. Biophys. Bioeng. 3*, 179–201.

Edidin, M., & Fambrough, D. (1973) *J. Cell Biol. 57*, 27–53.

Edidin, M., Zagyansky, Y., & Lardner, T. J. (1976) *Science (Washington, D.C.) 191*, 466–468.

Fowler, V., & Branton, D. (1977) *Nature (London) 268*, 23–26.

Frye, L. D., & Edidin, M. (1970) *J. Cell Sci. 7*, 319–335.

Hoffman, W. F., Norisuye, T., & Yu, H. (1977) *Biochemistry 16*, 1273–1278.

Jacobson, K., Wu, E. S., & Poste, G. (1976) *Biochim. Biophys. Acta 433*, 215–222.

Koppel, D. E. (1979) *Biophys. J. 28*, 281–291.

Koppel, D. E., Sheetz, M. P., & Schindler, M. (1980) *Biophys. J. 30*, 187–192.

Liebman, P. A., & Entine, G. (1974) *Science (Washington, D.C.) 185*, 457–459.

Matsumoto, M., Watanabe, H., & Yoshioka, K. (1970) *J. Phys. Chem. 74*, 2182–2188.

Norisuye, T., & Yu, H. (1977) *Biochim. Biophys. Acta 471*, 436–452.

Norisuye, T., Hoffman, W. F., & Yu, H. (1976) *Biochemistry 15*, 5678–5682.

O'Konski, C. T. (1976) *Molecular Electro-Optics*, Marcel Dekker, New York.

Peters, R., Peters, J., Tews, K. H., & Bahr, W. (1974) *Biochim. Biophys. Acta 367*, 282–294.

Poo, M.-M., & Cone, R. A. (1974) *Nature (London) 247*, 438–441.

Poo, M.-M., & Robinson, K. R. (1977) *Nature (London) 265*, 602–605.

Poo, M.-M., Lam, J. W., Orida, N., & Chao, A. W. (1979) *Biophys. J. 26*, 1–21.

Record, M. T., Jr., Anderson, C. F., & Lohman, T. M. (1978) *Q. Rev. Biophys. 11*, 103–178.

Schindler, M., Koppel, D. E., & Sheetz, M. P. (1980) *Proc. Natl. Acad. Sci. U.S.A. 77*, 1457–1461.
Schlessinger, J., Koppel, D. E., Axelrod, D., Jacobson, K., Webb, W. W., & Elson, E. L. (1976) *Proc. Natl. Acad. Sci. U.S.A. 73*, 2409–2413.
Singer, S. J., & Nicolson, G. L. (1972) *Science (Washington, D.C.) 175*, 720–731.
Smith, B. A., & McConnell, H. M. (1978) *Proc. Natl. Acad. Sci. U.S.A. 75*, 2759–2763.
Smith, H. G., Jr., Stubbs, G. W. & Litman, B. J. (1975) *Exp. Eye Res. 20*, 211–217.
Tabor, C. W., & Tabor, H. (1976) *Annu. Rev. Biochem. 45*, 285–306.
Tabor, H., Tabor, C. W., & Rosenthal, S. M. (1961) *Annu. Rev. Biochem. 30*, 579–604.
Takezoe, H., & Yu, H. (1981a) *Biophys. Chem. 13*, 49–54.
Takezoe, H., & Yu, H. (1981b) *Biophys. Chem.* (in press).
Tinoco, I., Jr. (1955) *J. Am. Chem. Soc. 77*, 4486–4489.
Tinoco, I., Jr., & Yamaoka, K. (1959) *J. Phys. Chem. 63*, 423–427.
Wilson, R. W., & Bloomfield, V. A. (1979) *Biochemistry 18*, 2192–2196.

Photoincorporation of Puromycin into Rat Liver Ribosomes and Subunits†

A. M. Reboud,* S. Dubost, M. Buisson, and J. P. Reboud

ABSTRACT: [^{3}H]Puromycin was covalently incorporated into rat liver ribosomes and isolated 40S and 60S subunits on irradiation at 254 nm. A study of the concentration dependence of this photolytic incorporation suggested that it arose from specific sites on isolated subunits but also from unspecific ones in the case of ribosomes, these sites being probably located on contaminant nonribosomal proteins. Puromycin was incorporated simultaneously into ribosomal proteins and rRNAs. The results from simultaneous one-dimensional and two-dimensional gel electrophoreses showed a small distribution of label among ribosomal proteins in 60S subunits and in 80S ribosomes, L10 being the most radioactive protein. Some antibiotics, which act on the peptidyltransferase center (amicetin and gougerotin), and also tetracycline competed with this labeling. Therefore, it was concluded that puromycin interaction with protein L10 occurred most likely at a functional site. In the case of free 40S subunits, labeling distribution among proteins was much wider. The possibility that proteins S3 and perhaps S23–24, which were significantly labeled in crude ribosomes too, also belong to a specific site interacting with puromycin is discussed.

Coopermann et al. (1975), Coopermann (1980), and Jaynes et al. (1978) reported a photochemical reaction of labeled puromycin with ribosomes and isolated subunits of *Escherichia coli* and especially with rRNAs and proteins located on both subunits. Labeling of these components was observed in puromycin-specific binding sites, in close vicinity to the peptidyltransferase center.

A similar study is carried out here, on the localization of puromycin-incorporation sites within rat liver ribosomes and subunits, and on the concentration dependence of this incorporation. Until now, very few affinity labeling studies have been carried out to locate components involved in the peptidyltransferase center of these ribosomes (Stahl et al., 1974, 1979; Czernilofsky et al., 1977; Böhm et al., 1979). The main advantage of the direct use of puromycin over these other experiments is that it excludes the introduction of an extraneous chemical moiety.

Materials and Methods

Puromycin dihydrochloride was obtained from Sigma. [8-^{3}H]Puromycin (5–5.7 Ci/mmol) and [^{14}C]phenylalanine (200 mCi/mmol) were purchased from Amersham.

Preparation of Ribosomes. Rat liver ribosomes consisting mainly of polysomes were isolated according to a method adapted from that of Moldave & Skogerson (1967). No attempt was made to remove nascent chains and numerous other factors, e.g., aminoacyl-tRNA and messenger RNA, because the washing of ribosomes by high concentrations of salt has a particularly dramatic effect on protein reactivity (Ghosh & Moore, 1979). Occasionally they are denoted as crude ribosomes to distinguish them from the washed ribosomes obtained after puromycin and high-salt treatment used by others in comparable studies (see Discussion). Isolated subunits used directly in photolabeling experiments or subunits prepared from ribosomes labeled with [^{3}H]puromycin were obtained as described by Madjar et al. (1977) using a method adapted from that of Blobel & Sabatini (1971).

Photolytic Incorporation of Pyromycin. Photolysis experiments were performed by using ribosomes and subunits (80 A_{260} units/mL either in 5 mM $MgCl_2$ (60S subunits and ribosomes) or in 2 mM $MgCl_2$ (40S subunits) in a buffer of 50 mM triethanolamine, pH 7.4, and 50 mM KCl. Samples (140 μL, 2-mm solution depth) previously incubated with puromycin, either alone or in conjunction with other antibiotics (4 °C, 30 min), were irradiated at 4 °C for the periods of time indicated with a low-pressure mercury lamp having a maximum output at 253.7 nm and producing 2.9×10^2 erg mm^{-2} s^{-1} at the distance of the sample (10 cm). Incident radiation doses were determined by ferrioxalate actinometry (Parker, 1953). Immediately after photolysis, the mixtures were usually precipitated with 2 volumes of ethanol; the pellets were then extensively washed and tested for radioactivity after incubation with 1 mL of tissue solubilizer (2 h at 50 °C). During preliminary experiments, procedures such as ethanol or trichloroacetic acid precipitation (4 °C), dialysis, and sedimentation through a sucrose cushion were tested in order to find the best method of excluding the noncovalent sticking label.

† From the Laboratoire de Biochimie Médicale, Université Lyon 1, 69622 Villeurbanne, France. *Received October 15, 1980; revised manuscript received April 21, 1981.* This work was supported in part by the Centre National de la Recherche Scientifique (ERA 399), the Institut National de la Santé et de la Recherche Médicale (78.1.59.3), and the Délégation Générale â la Recherche Scientifique et Technique (79.7.0160).

0006-2960/81/0420-5281$01.25/0